Chapter 1

Introduction

In recent days, modern communication has ushered in a paradigm shift in terms of frequency allocation diversity, characterized by vast impedance bandwidths, high device densities, low latency, and a massive number of transceiver antennas [1]-[5]. The exponential growth of wireless communication devices necessitates the development of low-profile antennas with enhanced bandwidth and gain [1]-[5]. Earlier, numerous techniques such as coplanar parasitic patches, stacked patches, dielectric resonators, and the incorporation of various types of slots were used to design and develop broadband antennas [4]-[7]. However, these antennas were large, complicated to design, along with a limited bandwidth [4]-[7]. As a result, the substantial design and development of dual-band antennas have conveyed numerous challenges to the advancement of modern communication systems hence, introducing various operating frequency ranges and numerous wireless standards [8]-[14].

This chapter discusses the theoretical backgrounds of two-dimensional (2D) metasurfaces, which are the surface representations of metamaterials [15]-[17]. Later in this chapter, typical metasurface antennas are studied, and their inherent limitations emphasize the advantage of integrating metasurface (MS) with the radiating element [18]-[31]. The MS can significantly improve the antenna performance in terms of impedance bandwidth, gain, and efficiency for different applications [18]-[31]. Additionally, this chapter provides an overview of the research objectives for the MS antennas. Finally, a summary of the original contributions is provided.

1.1 Metamaterial

Metamaterials (MTM) are engineered materials that are not natural and comprise subwavelength-scale repetitive patterns [32-34]. The arrangement of shape, size, geometry, the orientation of the repeating pattern gives them unusual features [32-34]. The wavelength must be substantially lower than the distance between these meta-atoms and their overall dimension [32-34]. Due to the granularity of the structure, a wave traveling through the medium does not suffer from diffraction or Bragg scattering [32-34].

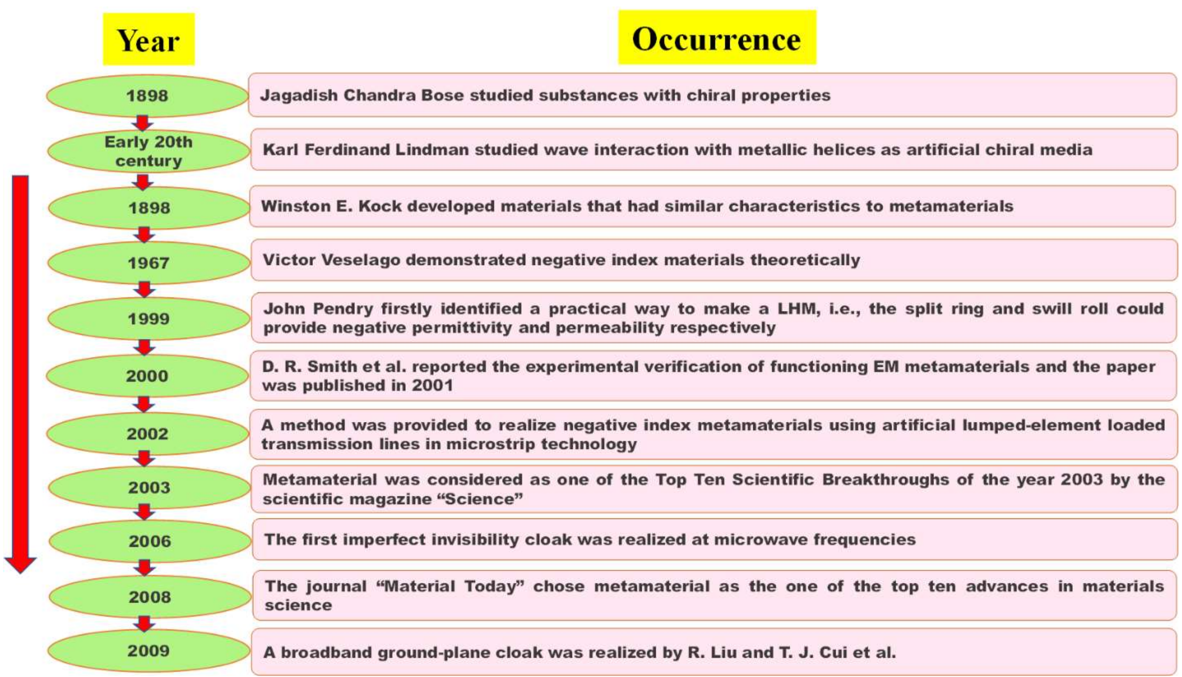

Fig. 1.1 The structural evolution of the metamaterials.

The term "metamaterial" was first invented by Rodger M. Walser in the context of a DARPA Workshop in 1999 [32-34]. The history and development of metamaterials are comprehensively documented in Fig. 1.1 [35-57]. It was proposed to characterize a class of artificial materials with superior electromagnetic properties to those found naturally. The metamaterial is derived from the Greek word "meta" (beyond), which means "beyond the material" [17, 32, 33]. Brown had previously investigated artificial materials with negative refractive index in the 1950s [39]. Then, in the 1960s, Rotman became interested in the electromagnetic properties of a wire medium analogous to plasma [40]. Veselago later predicted a whole new class of materials in 1968 [41], where both permittivity and permeability have negative values, resulting in a negative refractive index. Moreover, in the 1980s and 1990s, artificial materials such as microwave absorbers and bianisotropic media were developed [16, 33, 34]. Finally, in 2001, Smith [42, 43] experimentally produced a negative index of refraction, and later Pendry [44] reintroduced the concept of negative refraction (proposed by Veselago) to suggest the construction of a perfect lens. When Pendry and Smith conceived and realized the electromagnetic cloaking based on transformation optics in 2006, the scientific community became highly interested in the study of metamaterials [44-53].

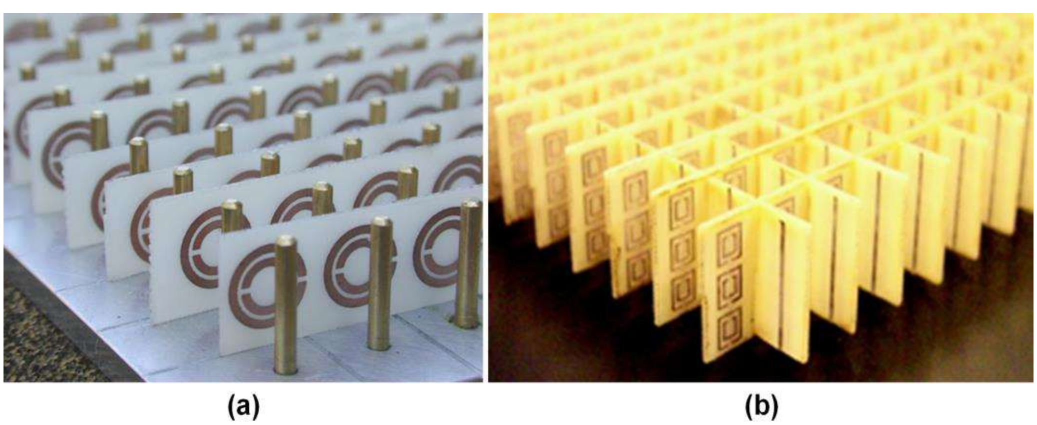

Fig. 1.2 First realized left-hand metamaterials (a) using circular rings (b) using square rings.

The metamaterial structure can then be homogenized to determine its corresponding effective material properties in this scenario [16-19]. The electromagnetic properties of the materials can be classified into four groups based on permittivity and permeability values, such as double-positive (DPS), epsilon-negative (ENG), mu-negative (MNG), and double-negative (DNG). In nature, DPS, MNG, and ENG values exist for dielectrics, magnetic materials, and plasmas, respectively [16-19].

A metamaterial with negative permittivity and permeability, also known as a negative refractive index (DNG), does not exist in nature and can only be created artificially [45-48]. They exhibit the characteristics of electromagnetic waves and are referred to as left-handed materials (LHM) [45-48]. In these types of metamaterial, the group and phase velocities are also reversed, and waves move in the opposite direction. Pendry published a paper in 1999 on employing split-ring resonators (SRRs) to build a medium with negative permeability [16]. Smith and colleagues regularly observed the metal lines and SRRs to demonstrate the negative refractive index in 2000 [45-48]. Since then, numerous studies have been conducted with outstanding outcomes [45-48]. Further, the negative refractive index materials using circular and square becomes popular which is represented in Fig. 1.2 [45-48]. However, those structures suffer from narrow bandwidth, substantial dispersion, and anisotropy. Further, they are challenging to implement and deploy in real-world implementations due to their significant losses [48-52].

Additionally, researchers focus on the metamaterials with further exceptional features, such as epsilon-near-zero (ENZ), mu-near-zero (MNZ), perfectly magnetic conductors (PMC), zero-index materials (ZIM), etc. [16-17]. These materials' effective permittivity and permeability can be exploited, simplifying their manufacture and application. In 1999, Sievenpiper et al. constructed a perfectly magnetic conductor (PMC) utilizing a high-impedance surface (HIS) with a periodic mushroom structure composed of patches and vias [16-17]. Later, other configurations with similar features to the HIS structure have been found, such as electromagnetic bandgap (EBG) and reactive impedance surfaces designs [16-17]. These structures are called "artificial magnetic conductors" (AMC). AMCs, in contrast to perfect electric conductors (PEC), do not exhibit a phase change when an electromagnetic wave is incident vertically and reflected toward the source. The image current generated in the AMC is parallel to the current flowing through the conductor of the AMC [16-17]. This physical process, known as constructive interference, can improve antenna qualities even when the antenna is positioned very close to the AMC, which can be very useful for antenna miniaturization and optimization [16-17]. Later, the two-dimensional structure of metasurfaces, in contrast to the three-dimensional design of normal metamaterials, allows them to be placed in smaller spaces [53-58]. In the first decade of the twenty-first century, there was a lot of interest in metamaterials for various uses. They became less popular because of their complexity, bulkiness, weight, and limitations in terms of the frequency range, loss, and scalability [53-58]. In recent days, the two-dimensional analogues of metamaterials such as metasurfaces attracted much interest in different practical applications, and the research field becomes exploded [59-60].

1.2 Metasurface

Metasurfaces are the two-dimensional arrangement of metamaterials or it is simply a surface distribution of electrical field scatters capable of manipulating and controlling electromagnetic waves [59-62]. The geometrical shape of the scatters generated on the dielectric substrate determines the functionality of the metasurfaces [59-62]. Metasurfaces have the unique properties of having an ultra-low profile and improved gain features with directive radiation pattern and a wider bandwidth [62-65]. Many other advantages of metasurfaces, including their low cost, light-weight, excellent flatness, and simplicity of manufacture, have led to the expansion of metasurface research from microwave to optical frequencies over the past decade [62-65]. MS has several potential uses, including antenna performance enhancement, reduction in the size of the resonator, reconfigurable antenna, controllable "smart" surfaces, etc. [63-65].

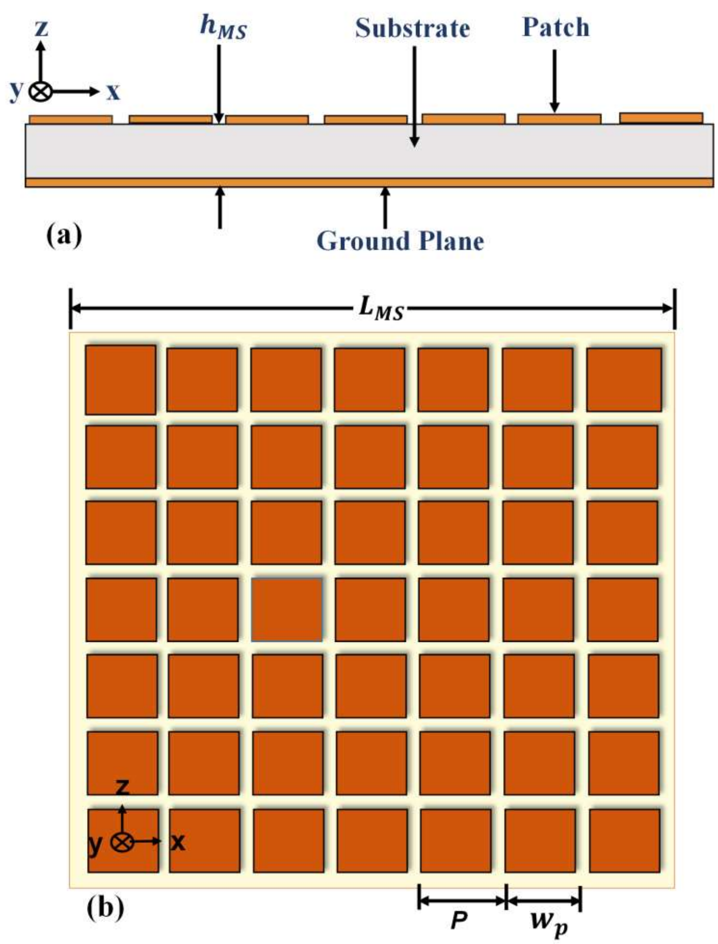

Fig. 1.3 A generalized metasurface structure (a) side view and (b) top view.

The metasurface structure depicted in Fig. 1.3 comprises squared-metal patches grouped regularly on a substrate. It has a metallic patch size of w_p and a periodicity of P. The surface wave resonances of a finite metasurface-based antenna can be estimated qualitatively using the equation (1.1), where β_{SW} is the propagation constant of surface wave resonances, and L_{MS} signifies the overall length of the MS structure as represented in (1.2)

$$\beta_{SW} \times L_{MS} = \pi \quad (1.1)$$

$$L_{MS} = N \times P \quad (1.2)$$

N and *P* are the numbers of cells and periodicity between the metasurface unit cells, respectively. Putting (1.2) into (1.1) yields (1.3)

$$\beta_{SW} = \frac{\pi}{N \times P} \quad (1.3)$$

The expression in (1.4) relates the decay constant α and the angular frequency ω

$$\beta_{SW} = \sqrt{\eta^2\omega^2 + \alpha^2} \quad (1.4)$$

For transverse electric (TE) and transverse magnetic (TM) waves, the propagation constant can be determined from (1.5-1.6) respectively,

$$\beta_{TM} = \frac{\omega}{c}\sqrt{1 - \frac{Z_S^2}{\eta^2}} \quad (1.5)$$

$$\beta_{TE} = \frac{\omega}{c}\sqrt{1 - \frac{\eta^2}{Z_S^2}} \quad (1.6)$$

where $\beta_{TM}$and β_{TE} denote the propagation constants of TM- and TE-waves, respectively, c signifies the speed of light in a vacuum, while η and Z_s represent the intrinsic and surface impedances of the metasurface structure respectively.

1.3 Metasurface Antenna

In recent times, different kinds of convenient radiating antennas are designed using MS. Each design consists of an MS and a simple antenna, such as a patch or slot antenna [20-31]. The characteristics of patch antennas and slot antennas are discussed in this section [66-68].

Numerous low-profile MS antennas with much greater performance than conventional antennas have been built and explored [69-76]. MS can be used to tune the surface impedance, regulate the reflection coefficient phase, manipulate the propagation of surface waves, control the frequency band, control edge diffractions, and control the radiation patterns of antennas [69-76]. One significant difficulty with metasurface antennas is the occurrence of resonances other than the typical resonance induced in the main radiating element due to the occurrence of MS structure with finite size [66-68]. This thesis uses MS to design various antennas, including miniaturized patch antennas, slot antennas, CPW-Fed antennas, and dual-band antennas. At the same time, MS can significantly improve antenna performance in terms of impedance bandwidth, gain, and efficiency [69-76].

1.3.1 Design Analysis

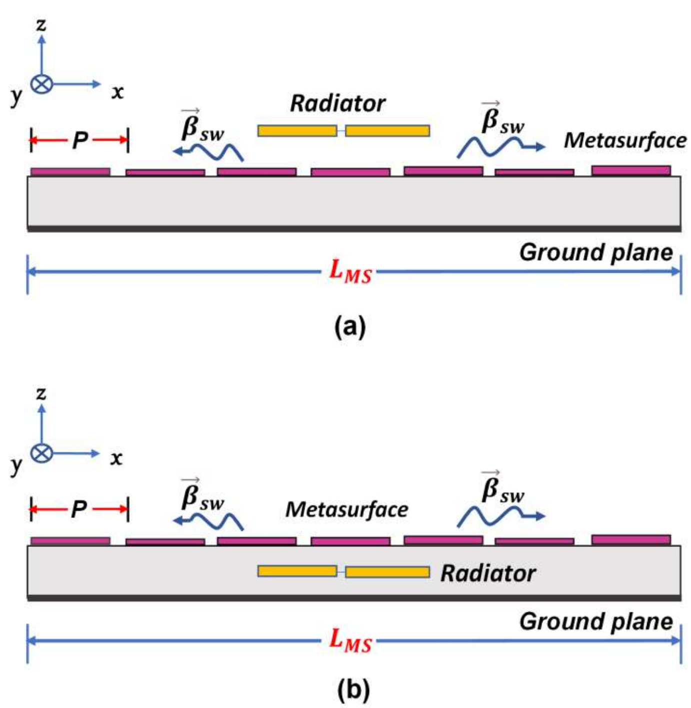

Fig. 1.4 Radiating element arrangement in an MS antenna (a) radiator above MS (b) radiator below MS.

An antenna is a device that converts electrical power to broadcast electromagnetic waves (and vice versa). To put it another way, the antenna is a bridge between free space and a directing device. Several metrics have been developed to describe antenna performance, including bandwidth, radiation pattern, beamwidth, directivity, gain, antenna efficiency, polarisation, axial ratio, and sidelobe level [66-68]. The primary radiating elements such as microstrip patch antennas, and horizontal dipoles generate additional resonances on a finite-sized MS structure [77-78]. Surface waves traveling through the metasurface structure provide this additional resonance, as illustrated in Figs. 1.4(a) and 1.4(b). Depending on the application, the driven radiator can be positioned either above or below the MS. During resonances, the overall length of the metasurface is equal to the resonant length of a specific surface wave [77-78]. As a result, additional resonances in an antenna configuration are formed by diverse waves.

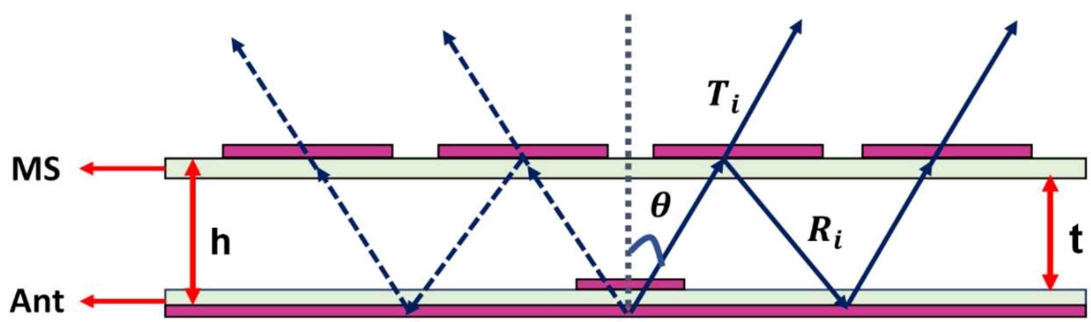

Fig. 1.5 The architecture of conventional MS antenna in which electromagnetic waves from the source antenna can be partially transmitted and reflected by the metasurface.

The architecture of a standard MSA with their working analysis is shown in Fig. 1.5, where the MS is superimposed on a primary element. The radiated electromagnetic wave from the source antenna may be partially reflected and transmitted as a result of the MS. Multiple reflections and transmission waves with diminishing amplitudes are formed between the ground and MS. According to the ray theory presented in [77-78], the electric field in the far-field region is the vector sum of these partially transmitted rays, which can be represented in (1.7)

$$E_T = \sum_{i=-\infty}^{\infty} f(\theta) E_i \qquad (1.7)$$

$$E_i = E_0 T e^{j\psi T_i} \qquad (1.8)$$

Here, $f(\theta)$ the function of the source's radiated field pattern with respect to the angle of incidence θ and E_i in (1.8) represents the resultant of the successive reflected field vectors during reflections from the ground layer and MS, E_0 denotes the amplitude of the electromagnetic wave from the source, ψT specifies the transmission phase of the MS, and *i* is the transmitted wave index. If the resonance condition in (1.9) is satisfied, then the power is radiated in the broadside direction,

$$\psi - \pi - \frac{4\pi h}{\lambda_0} = 2N\pi \qquad (1.9)$$

Here *N* specifies as an integer, and λ_0 represents the free-space wavelength. As a result, the height (*h*) is found to match the requirements provided in (1.10) for the resonance distance:

$$h = \left(\frac{\psi}{360} - 0.5\right)\frac{\lambda_0}{2} - N\frac{\lambda_0}{2} \qquad (1.10)$$

The antenna radiates with high directivity toward the broadside when the MS is made up of homogenous unit cells. The MSA, on the other hand, may radiate at an angle offsets from the broadside if the MS is designed with nonhomogeneous unit cells with a gradient phase.

1.3.2 Analysis of the Unit Cell

The analytical Drude-Lorentz model or the S-parameter retrieval method [47-49] can be used to analyze electromagnetic properties such as complex permeability (μ) and the permittivity (ε). The S-parameter extraction method has been employed. The reference planes of the two ports must adhere to the unit cell, which may be seen in the side view of the simulation setup. The comparable relative permittivity ε_r and permeability μ_r may be calculated using the values of S_{11} and S_{21}. First, using (1.11) and (1.12) from [47-49], the equivalent impedance Z and the reflective index n of the MS are always determined.

The S-parameters of the system can also be indicated in equations (1.11-1.12)

$$S_{11} = \frac{R_{01}(1-e^{i2nk_0d})}{1-R_{01}^2 e^{i2nk_0d}} \tag{1.11}$$

$$S_{21} = \frac{(1-R_{01}^2)e^{i2nk_0d}}{1-R_{01}^2 e^{i2nk_0d}} \tag{1.12}$$

Solving equations (1.11) and (1.12) provide

$$z = \pm\sqrt{\frac{(1+S_{11})^2-S_{21}^2}{(1-S_{11})^2-S_{21}^2}} \tag{1.13}$$

$$e^{ink_0d} = \frac{S_{21}}{1-S_{11}\frac{z-1}{z+1}} \tag{1.14}$$

$$n = \frac{1}{k_0d}\left[\left\{\left[ln\left(e^{ink_0d}\right)\right]'' + 2m\pi\right\} - i\left[ln\left(e^{ink_0d}\right)\right]'\right] \tag{1.15}$$

Where $(.)''$ and $(.)'$ denote the real and complex components, respectively; S_{11} and S_{21} are reflection and transmission coefficients, respectively; R_{01} is $\frac{z-1}{z+1}$; z in (1.13) represents the normalized impedance; the refractive index n is calculated using (1.14) and is represented by the equation (1.15); k_0 is the wavenumber; d denotes the maximum length of the unit element, and m signifies the branch caused by the sinusoidal function's periodicity [48]. Additionally, permittivity (ε) and permeability (μ) are proportional to refractive index and normalized impedance as shown by the formulas (1.16-1.17)

$$\varepsilon = \frac{n}{z} \tag{1.16}$$

$$\mu = nz \tag{1.17}$$

1.3.3 Other Parameters for Metasurface Antenna Design

Transmission lines, such as electrical power lines, waveguides, and conducting wires, are structures that direct the transmission of signals or energy from one location to another [66-67]. In practice, appropriate connectors like BNC, SMA, and type N connectors [66-67] are required to facilitate the coupling of transmission lines and associated devices. The SMA connectors are employed in our experimental work in this thesis. Different transmission lines have been designed for a wide range of purposes. Microstrip, coaxial, and coplanar waveguides (CPW) are prominent examples in antenna and RF engineering [66-67]. The bandwidth, impedance, and basic mode properties of these transmission lines are addressed in this section.

A. Microstrip Line

A microstrip line is a type of planar transmission line that is widely utilized in many applications. In a microstrip transmission line, the characteristics impedance depend upon the permittivity as well as the ratio of *w/t*; where *w* is the width of the microstrip line and *t* is the thickness of the substrate. The impedance decreases as the permittivity and *w/t* ratio increase. Industrial standard lines typically have a characteristic impedance of 50 or 75 ohms [66-67]. For compatibility with SMA connectors, the characteristic impedance of the microstrip line and the CPW will be maintained at 50 Ω throughout the next parts of this thesis.

B. Co-axial Cable

Coaxial cables are made of two concentric conductors: an inside conductor and an exterior conductor that is tubular in shape. Inner and outer conductors are often separated by dielectric materials that act as insulation between them. It appears that the E-field and H-field are located in a transverse plane within the cable, indicating that it is in TEM mode. It is possible that the TEM field contained within the coaxial wire has been lost. The existence of higher modes such as TE_{11} (in which only the E-field occurs in the transverse plane and the H-field has no non-transverse component) is undesirable since the loss increases [66-67].

C. Co-planar Waveguide

An evolution of coaxial cable results in the formation of a co-planar waveguide (CPW) structure. In this configuration, the center conductor is isolated from two ground planes that are positioned on the same side of the substrate. CPW is widely used because of its several benefits, including its ease of fabrication and integration into circuits, and its ability to provide strong circuit isolation at extremely high frequencies (100 GHz or higher) [66-67].

D. Patch Antenna

Patch antennas are low-profile, adaptable to both planar and non-planar structures, and simple to construct. Patch antennas are basically composed of a rectangle or square metal patch affixed to a thin dielectric substrate [66-67]. The metal ground plane is located on the bottom side of the substrate. Depending on the application, antenna patches can be constructed in a variety of shapes and sizes. Patch antennas are gaining popularity, particularly for frequencies exceeding 100 MHz. Patch antennas suffer from poor power handling capability, which makes them unsuitable for high-power applications, as well as a narrow impedance bandwidth. However, great progress has been made in extending the bandwidths of patch antennas, for example, through stacking and other techniques, in order to fulfill the growing demand of the wireless communications sector [66-67]. Recently, substantial emphasis has been made to reconfigurability of patch antennas via the addition of loads, switches, or the use of metasurface, all of which are described in greater detail in the next chapters.

D. Slot Antenna

The slot antenna offers a wide range of practical uses due to its low profile and versatility [66-67]. A slot in a metal plate or waveguide offers identical radiation pattern as a driven rod antenna with the same shape [66-67]. Magnetic dipoles have a field that runs parallel to the broader side of the slot axis and an electric field that flows perpendicular to that field. The same equations that apply to a dipole can be used to estimate the radiation pattern of a slot. The waves are linearly polarised in the slot. It is common to practice to employ array antennas that have numerous parallel slots in a waveguide. Linear arrays of dipole antennas radiate in a similar fashion, however, the slot can only radiate into the surrounding area on one side of the waveguide area [66-67].

1.4 Metasurface Synthesis and Circuit Model

Metasurfaces are gaining popularity due to their ease of manufacture and wide range of practical applications [79-81]. A propagating wave encounters discontinuity when an MS is present. The analysis of an MS can also be done by using a circuit model, where the MS is represented as a shunt impedance in the study [79-81]. The reactance X describes the inductive or capacitive behavior of the periodic surface, while the real part of the equivalent impedance R accounts for ohmic losses in the metal and dielectric layers. The MS reflection and transmission coefficients (S_{11} and S_{21}) can be determined using typical transmission line relations as provided in (1.18-1.19), respectively

$$S_{11} = \frac{AZ_0+B-CZ_0^2-DZ_0}{AZ_0+B+CZ_0^2+DZ_0} \tag{1.18}$$

$$S_{21} = \frac{2Z_0}{AZ_0+B+CZ_0^2+DZ_0} \tag{1.19}$$

where *A, B, C, D* represents the parameters of the ABCD matrix of the model comprising the MS. The ABCD matrix is mentioned in (1.20)

$$\begin{bmatrix} A & B \\ C & D \end{bmatrix} = [M_1] \cdot \ldots \cdot [M_n] \cdot [M_{MS}] \cdot [M_{n+1}] \cdot \ldots \cdot [M_N] \tag{1.20}$$

Here, *M* are the ABCD matrix of every layer, N is the generic number of the dielectrics and n represents the nth dielectric substrate. The each layer for nth order element and for MS are represented in (1.21-1.22)

$$[M_n] = \begin{bmatrix} \cos(k_{zn}d_n) & jZ_n \sin(k_{zn}d_n) \\ j\frac{\sin(k_{zn}d_n)}{Z_n} & \cos(k_{zn}d_n) \end{bmatrix} \tag{1.21}$$

$$[M_{MS}] = \begin{bmatrix} 1 & 0 \\ 1/Z_{MS} & 1 \end{bmatrix} \tag{1.22}$$

where Z_{MS} is the approximate MS impedance computed from retrieved LC parameters. $Z_n^{TE} = \frac{(\omega\mu_r\mu_0)}{k_{zn}}$; $Z_n^{TM} = \frac{k_{zn}}{(\omega\varepsilon_r\varepsilon_0)}$ are the characteristic impedance of the dielectric layer for TE and TM polarization respectively, $k_{zn} = \sqrt{\epsilon_r k_0^2 - k_t^2}$ is the wavenumber and $k_t = k_0 sin(v)$ is the transverse component of the wavenumber with v corresponding to the normal incidence angle of the incoming wave and k_0 is the free space propagation constant. The quantities ϵ_0,ϵ_0, μ_0 and μ_r are the free space and relative dielectric permittivity and magnetic permeability respectfully.

A periodic unit cell can be built by an unlimited number of geometries. Certain geometries are more popular than others and are also straightforward to comprehend and manipulate [79-81]. It is proved that the MS reactance expression obeys Foster's theorem, implying that it has the identical pole-zero analytic features as a passive LC network. The quantity of lumped elements is proportional to the number of resonances [79-81].

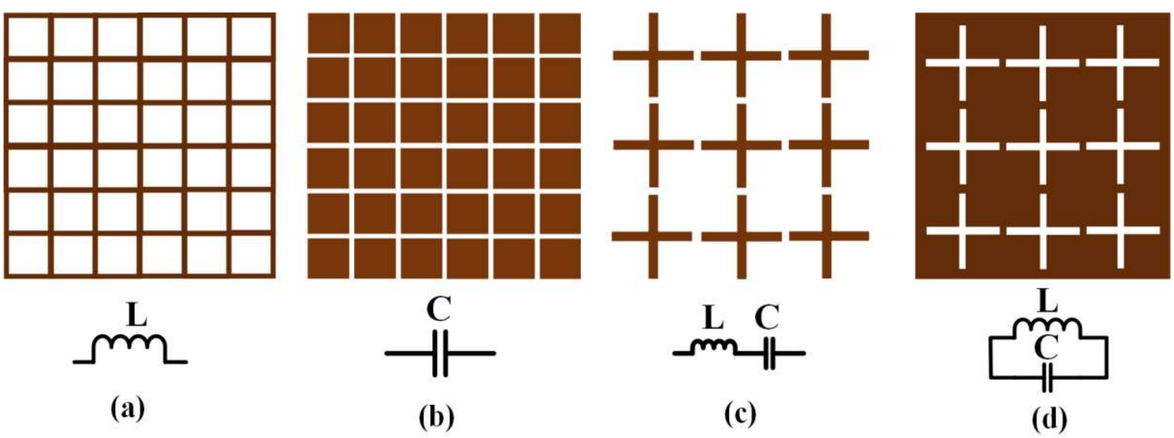

Fig. 1.6 Various MS elements and associated circuit models (a) inductive grid (b) Capacitive patch (c) capacitive cross and (d) inductive cross.

TABLE 1.1: Metasurface Elements Classification and circuit model topology

Element Type	Element Shape	Equivalent Circuit
Non-resonant elements	Strip, patch, wire grid	C
Single-resonant	Loop, dipole, cross, tripole	(LC)
Double-resonant	Double cross, cross frame, double loop, Jerusalem cross, etc.	(LC)//(LC) or (LC)(L//C)
Multi-resonant	Concentric loop, Fractal elements, quadrifilar spiral, meandered dipole	(LC)//(LC)//(LC)….
Other	Split ring, cut loop	-

Various MS elements with their equivalent circuit representation are shown in Fig. 1.6. The impedance of basic nonresonant devices such as wire grids or patch arrays is primarily inductive or capacitive. When a resonant element is utilized instead of a solely capacitive or inductive one, a simple LC circuit can be used to fit the frequency response of an MS [60-62]. For capacitive metasurfaces, the circuit will be series inductive, whereas an inductive MS will use a shunt LC configuration. The metasurface impedance is totally imaginary in the absence of losses and is represented by two lumped parameters. Losses can be added into an equivalent circuit by introducing a series resistance [79-81]. Table 1.1 present the classification of the most common geometries on the basis of resonant characteristics and equivalent circuits [79-81].

1.5 Literature Survey

In this section, various metasurface antenna design methodologies with their performance improvement have been discussed [82-109]. The significant characteristic of MSAs is their ability to develop resonances from the metasurface structure in addition to the radiator resonances. This is particularly true for high-gain antennas [82-109]. Depending on the application, these extra resonances are utilized to improve the operative bands or overall bandwidth of the antennas. Generally, planar antennas are conformable, low-profile, simple to integrate, and inexpensive to manufacture [69-76]. However, they have poor directivity and excitation capability of surface waves, which conflicts with the system requirements [69-76]. Numerous attempts have been developed to cater the improvement of the performance of planar antennas, including electromagnetic band-gap materials (EBGs), artificial magnetic conductors (AMCs), resonant layers, fabry-perot (FP) cavities, and, most recently, metasurfaces [82-109]. It is highly desirable and encouraged to employ one of the methods described above to improve the performance of planar antennas while simultaneously achieving multi-functionality. These types of configurations can be used to examine antennas with spatial diversity and a wide range of operating frequencies in order to determine the new possibilities in a variety of practical applications, such as wireless communications. In addition, incorporating a thin MS-designed structure near the antenna improves the radiation characteristics of planar antennas. Moreover, near-field coupling between the antenna and the MS enhances the radiating area of the antenna while maintaining its profile, which is advantageous in certain circumstances [82-109].

1.5.1 Antenna with radiating element and metasurface on the same surface

The development of planar magneto-electro-dielectric waveguided metamaterials (MED-WG-MTM) for effective permeability and permittivity extraction is described in Fig. 1.7 [110]. The MEDWG-MTM cell has an electric complementary spiral ring resonator (CSR) in the upper metallic layer and a magnetic embedded Hilbert line (EHL) in the ground plane.

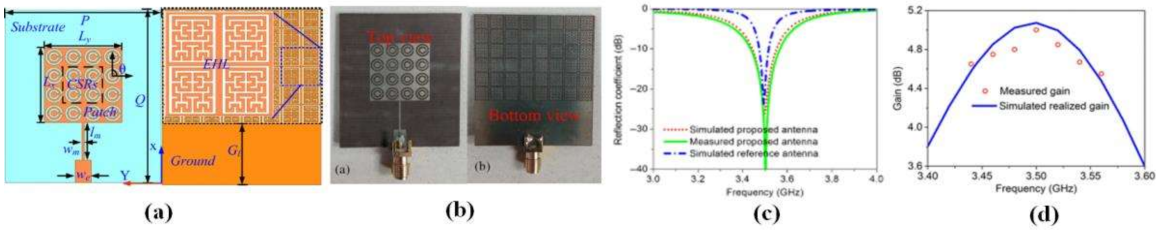

Fig. 1.7 (a) Antenna prototype (b) Fabricated structure (c) Reflection characteristics (d) Gain characteristics [110].

The electro-dielectric and magneto-dielectric waveguided substrates are combined to form a magneto-electro-dielectric waveguided MTM element, which is electrically smaller [110]. An upper metallic layer and a lower ground plane make up the planar WG-MTM artificial material in the planar waveguide environment. A two-turn complementary spiral ring resonator (CSR) was etched in the upper metallic plane, while an embedded Hilbert-line (EHL) inspired by the space-filling property of fractal curves was employed in the lower ground plane. Higher refractive index and wave impedance values are achieved by the proposed MTM element, which can be employed to reduce antenna size and boost antenna impedance bandwidth, respectively. The recommended antenna is less sensitive to metal shielding than a monopole antenna, regardless of operating band or BW, allowing for more practical applications.

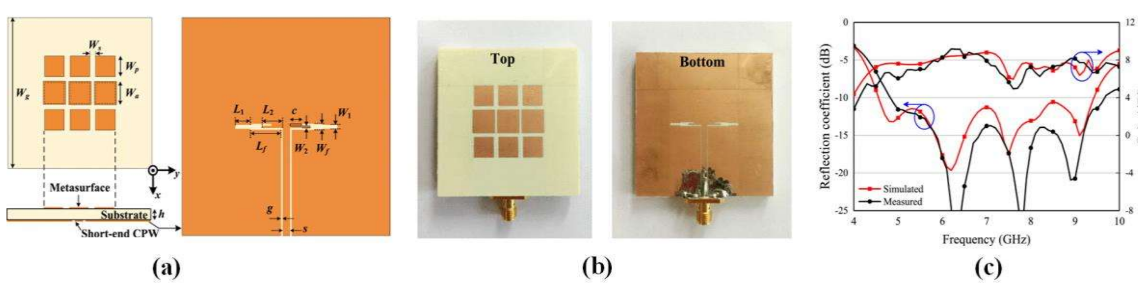

Fig. 1.8 (a) Antenna prototype (b) Fabricated structure (c) Reflection and Gain characteristics [111].

The second concept in Fig. 1.8 employs an aperture coupling to feed a single-layer broadband MS antenna through a coplanar waveguide (CPW) [111]. An MS radiator is fed by a stair-shape aperture on the bottom, which is again fed by a CPW amplification source. The antenna's input impedance can be adjusted for wideband characteristics using a special stair-shape aperture built for this purpose. The benefits of this antenna design include a wide impedance bandwidth, a single-layer structure, and ease of design and manufacture. The use of MS with radiating elements resulted in a wide impedance bandwidth of 67.3 % (4.81–9.69 GHz) and a maximum gain of 9.18 dBi.

1.5.2 Antenna with the radiating element below the metasurface

A method for developing planar antennas with sub-wavelength profiles and significant gain over a wide bandwidth is described in Fig. 1.9 [112]. An innovative multi-layer periodic array design is developed to increase the bandwidth performance of subwavelength fabry-perot cavity-type antennas. Three double-sided periodic arrays are constructed and optimized using an inductive partially reflected surface (PRS) and a capacitive artificial impedance surface (AIS) printed on either side of a dielectric substrate.

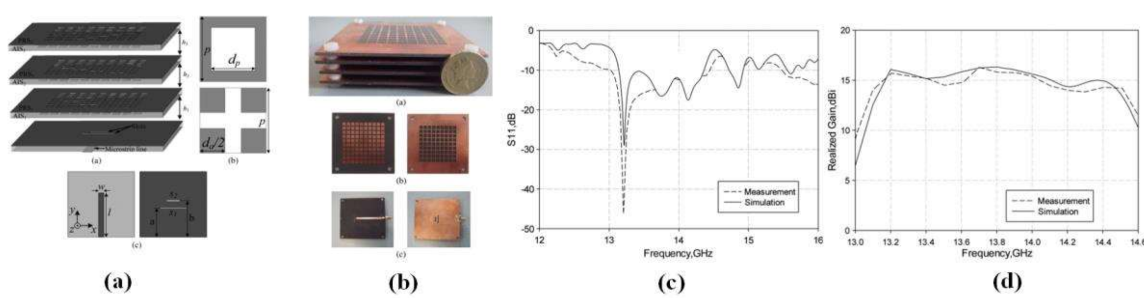

Fig. 1.9 (a) Antenna prototype (b) Fabricated structure (c) Reflection characteristics (d) Gain characteristics [112].

The distance between them and the ground plane is approximately one-sixth of a wavelength. A total profile of λ/2 is accomplished by establishing three air spaces in this manner. The proposed antenna has achieved 16.9 dBi directivity and 10.7 % of fractional bandwidth over a range of frequencies.

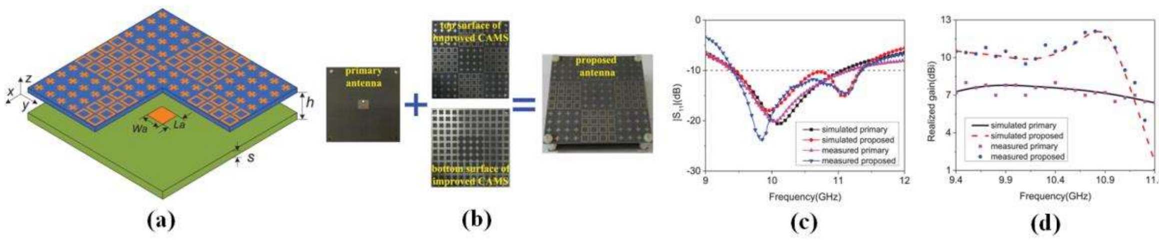

Fig. 1.10 (a) Antenna prototype (b) Fabricated structure (c) Reflection characteristics (d) Gain characteristics [113].

The next design techniques in Fig. 1.10 [113] demonstrates that an FP resonator antenna is capable of simultaneously increasing gain and decreasing the radar cross section (RCS). However, the absorption in the operational band is lowered to maintain the same radiation performance. As a result, RCS reduction inside the band is limited. In addition, the lumped resistance restricts applications that require the superstrate design to be smooth and oscillate. Another innovative superstrate is proposed to overcome the foregoing constraints. A checkerboard-organized metamaterial superstrate (CAMS) is composed of two distinct types of frequency selective surfaces (FSS) and is based on the RCS-reducing principle of chessboard reflection screens and the gain-enhancing theory of FP resonator antennas. The upper surface of CAMS has a chessboard-style layout that reduces RCS. To increase antenna gain, an FP resonator cavity is formed on the bottom surface of the primary antenna's ground plane. The FP resonator antenna enhances gain by 4.9 dB at 10.8 GHz and has a 3 dB gain bandwidth between 9.4 and 11.1 GHz (16.58%). Additionally, the suggested RCS of the FP resonator antenna is reduced from 8 to 18 GHz, resulting in a peak reduction of 39.4 dB. Additionally, the in-band RCS is significantly reduced as a result of the combined action of CAMS and the FP resonator cavity.

1.5.3 Antenna with the radiating element above the metasurface

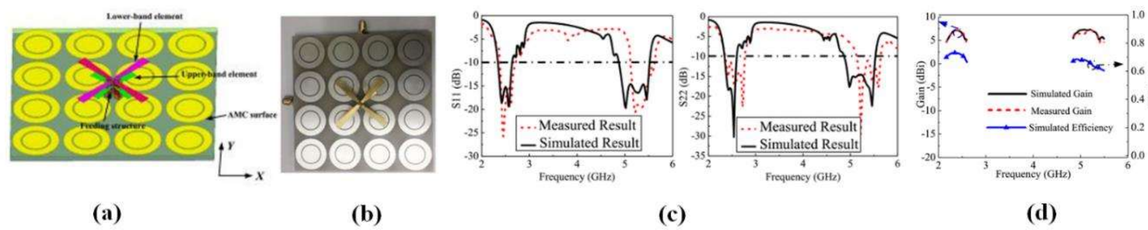

Fig. 1.11 (a) Antenna prototype (b) Fabricated structure (c) Reflection characteristics at port1 and port2 (d) Gain characteristics [114].

An antenna with an artificial magnetic conductor (AMC) surface for wireless local area network (WLAN) applications was shown in Fig. 1.11 [114]. Bowtie-shaped patches with U-slots and a 4x4 AMC surface are used to make this antenna. The bowtie shapes are responsible for wider bandwidth whereas the AMC surface improves antenna radiation characteristics. The radiation pattern of the antenna will improve as the number of AMC cells rises. While a lower reflector size can create edge-effect radiation, it can also cause the front-to-back ratio to be lowered, as well as impedance matching to be inadequate. This antenna is capable of functioning in two bands for WLAN applications, a lower band between 2.36 and 2.76 GHz and a higher band between 5.12 and 5.62 GHz. This antenna prototype generates radiation patterns with a peak gain of 7.2 dBi in the lower band and 7.3 dBi in the upper band. The proposed antenna is suitable for usage in multiband base stations for WLAN and other wireless networks.

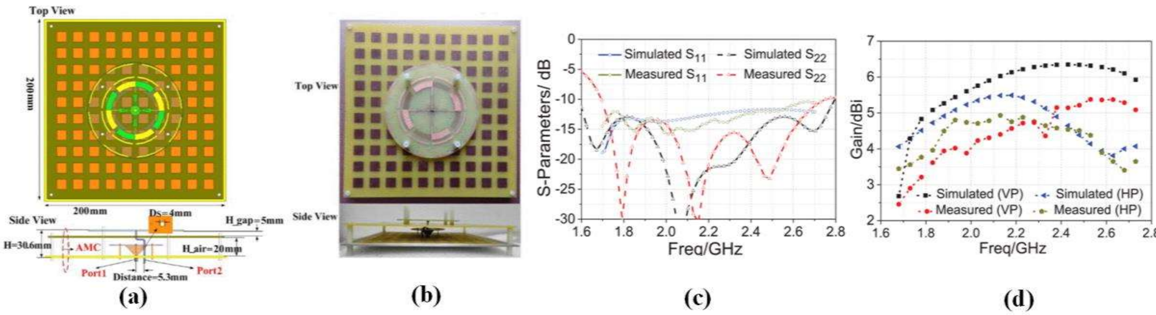

Fig. 1.12 (a) Antenna prototype (b) Fabricated structure (c) Reflection characteristics (d) Gain characteristics [115].

A dual-polarized, omnidirectional, wideband, and low-profile antenna with an artificial magnetic conductor (AMC) reflector is presented in Fig. 1.12 [115]. The antenna construction comprises of a vertically-polarized low-profile monopole antenna, horizontally polarized circular loop antenna, and an AMC reflector. Incorporating a circular ring, metallic reflector considered as a monopole, and AMC surface improves the antenna performance and makes the antenna directive at boresight direction. This antenna operates in the frequency range 1.7–2.7 GHz, has a 45% impedance bandwidth, and offers consistent radiation patterns. In order to achieve the desired antenna gain and bandwidth, a wider metallic ground plane with a thicker profile thickness is used in this antenna.

However, the MS antennas reported in [110-115] are developed on dielectric substrates with larger dimension as well as permittivity. Additionally, the antenna designs are little complex, and the profile thickness are quite large. Nowadays, modern communication systems necessitate portable, light-weight, low-profile antennas that are highly efficient and have a small profile thickness. As a result, antenna miniaturization with improved performance is quite challenging for antenna designers. This thesis discusses some efficient low-profile MS antennas for various practical applications.

1.6 Motivation of the Thesis

Modern communication has shifted dramatically in the last few days across multiple frequency bands as a result of large impedance bandwidths, high device density, low latency, and proliferation of transceiver antennas. [83-95]. Researchers and engineers have begun to pay more attention to small and inexpensive dual or multiband antennas because of their frequency reusability and enhanced channel bandwidth, owing to the rapid growth of existing wireless communication systems [83-95]. In particular, metasurface antenna (MSA) can meet a wide range of criteria depending on wireless communications applications compared to other antennas [96-99]. Additionally, by deploying MSAs, the constraint on the relative position of transmitting and receiving antennas can be eased, lowering the possibility of unreliable wireless disruptions in the network [96-99]. According to the preceding, compact MSAs with multiple operational frequency bands are attractive options for integration into modern communication systems [100-103]. Generally, metasurfaces (MS) are manufactured surfaces with unique electromagnetic properties not found in nature. MS structures exhibit flexible reflection characteristics and controllable dispersion characteristics in various applications, including absorbers, polarisation converters, antennas, filters, etc. [16-17]. The MSA structure can be employed in multiple applications, including imaging, wireless, optical communications, and aerospace [96-109]. The metasurface-embedded antenna designs can produce highly directive radiation patterns with far-field characteristics [96-100]. In recent times, various devices such as high impedance surfaces (HIS), electromagnetic bandgap (EBG) structures, and artificial magnetic conductors (AMC) have been developed using the features of MS [103-108]. This thesis discusses the synthesis and development of metasurface antennas for various practical applications. The main features of MSAs are their simplicity combined with beam control capabilities for shaping, directing, and scanning and their adaptability to a wide variety of technologies. Additionally, the MS antennas feature a small envelope, low mass, high gain with directional radiation characteristics, and limited power losses [96-109]. They have set up applications in various fields, viz., satellite communication, medical diagnosis, defense, wireless applications, etc. [96-109].

1.7 Thesis Contribution and Organization

The thesis consists of six chapters. Chapter one is the introduction part, where the straightforward concept of the metasurface is given, followed by a review of the recent research and development in this dynamic field. This chapter reviews the current progress of metasurfaces and their applications in the GHz domain. The theory and design analysis of the MSA is involved in this Chapter. Given that the main work of this thesis is experiment-based, a brief discussion about the sample fabrication is presented as well. Chapter two to five discusses in detail the research work done by the candidate and his co-workers. The second chapter focused on the design and analysis of a single-layered compact metasurface antenna capable of increasing the impedance bandwidth. A superstrate-based MSA is being used in chapter three, which improves the gain to a significant level. Chapter four discusses a compact, dual-band metasurface antenna with its respective circuit model, verifies the results. Further, in chapter five, an AMC-based MS antenna has been proposed for WLAN along with modern civil and military applications. The design analysis, simulation, sample fabrication, and experimental results are given in detail in each of these four chapters. In the last chapter of the thesis, all the works have been summarized with the scope of future studies.

The first chapter provides an overview of metasurfaces and their applications. Later, traditional metasurface antennas are reviewed, and their fundamental limitations bring up the motivation that incorporating MS with the radiating element enhances their performance. This thesis presents and discusses the mathematical formulation, practical realization, applications, and concepts of metasurface antenna.

In Chapter 2, a new, modified, portable, dual, and wideband metasurface (MS) antenna with high gain is proposed. Increasing the antenna's bandwidth using a typical microstrip patch with a compact dimension is pretty challenging. However, bandwidth and gain can significantly increase by incorporating a metasurface into the ground plane while keeping compactness. The MSA consists of a source antenna (a conventional planar antenna such as a slotted patch antenna) and a 4×5 periodic metasurface in the bottom of the dielectric adjacent to the partial ground. Each unit cell is composed of a periodic arrangement of two L-type patches and a cantered C-type patch. MS antennas are constructed and measured to validate the simulation results. The findings of the simulations and measurements are in good accord. The results indicate that the MS antennas outperform the source antennas in terms of gain, impedance bandwidth, and radiation pattern.

Chapter 3 is a continuation of Chapter 2, in which the gain and radiation characteristics of the antenna are improved. The 5×5 order MS is placed directly atop the patch antenna, acting as a superstrate, resulting in a compact and low profile MSA. The patch employs fractal geometry and dielectric via to change the operating frequency to the desired frequency range [8-14]. By incorporating two rectangular slots in the ground plane, the proposed prototype includes the defective ground approach. This diminishes surface waves, which in turn minimizes cross-polarized radiation [8-14]. Additionally, the slot in the microstrip patch has increased the impedance bandwidth and improved the cross-polarized radiation characteristics in the broadside direction [8-14]. The developed antenna operates in the X-band region, where the operational band can be tuned simply by altering the position of the dielectric via and the periodic slot dimensions. The prototype for the specified design has been fabricated and tested. The simulation and experiment results are substantially consistent.

Chapter 4 presents the design and analysis of MS antennas using multi-layered dielectric. Two separate source antennas have been used for different MS antenna designs. These structures can be easily implemented and controlled in new applications using a planar antenna. The first type employs split-ring resonators (SRRs) implanted in the square slots of the radiating patch. The MS is positioned with the slotted corner cut rectangular patch antenna in the same plane as a defective ground plane. The performance of the antenna has been improved by the addition of a 4×5 order metasurface to the upper section and two 1×4 cell arrays adjacent to the standard patch. An equivalent circuit model of SRR and the proposed unit cell have been discussed. Later, the circuit model for the proposed MSA was analyzed. The proposed antenna is single-layered, and offers broad impedance bandwidth along with high gain, with the feature of ease of fabrication. The measured results are in good agreement with the simulated ones. In the second design, a 7×7 order MS structure has been placed as a superstrate configuration just above the radiating element separated by an air spacer. The prototype offers satisfactory impedance bandwidths at C- and X- bands. The detailed circuit model analysis has been sequentially developed to validate the impedance behaviour of the proposed antenna configuration. The proposed prototype has been built, and the experimentally measured findings match the simulated results well.

In Chapter 5, an efficient, compact, wideband with improved gain and directional AMC-based MS antenna (MSA) has been presented for wireless applications. The MSA has been formed by sandwiching together a coplanar waveguide-fed (CPW-fed) slotted patch antenna and a 7×7 order metasurface (MS) in a stacked configuration. A Teflon material has been used to separate the AMC surface from the radiating patch. Here, the radiating element is placed on top of the first dielectric, while the MS layer has been positioned on top of the second dielectric. The proposed prototype has been fabricated, and the experimentally measured parameters are in good resemblance with the simulated values.

Chapter 6 summarizes and concludes the thesis and discusses future research directions.